Laser-assisted antihydrogen formation

A. Chattopadhyay and C. Sinha
Department of Theoretical Physics, Indian Association for the Cultivation of Science, Jadavpur, Kolkata 700032, India
(Received 6 March 2006; published 1 August 2006)

Laser-assisted antihydrogen ($\bar{H}$) formation cross sections (differential and total) for collisions of antiprotons with positronium (Ps) are studied in the framework of the eikonal approximation for two geometries, when the field polarization is parallel ($\|^L$) or perpendicular ($\perp^r$) to the incident Ps momentum. The variations of the $\bar{H}$ formation cross sections with respect to the field strength and the laser photon energy are studied for the multiphoton (absorption and emission) processes. The contribution of the atomic (both Ps and $\bar{H}$) dressing terms to the enhancement of the $\bar{H}$ formation cross section is studied for both the geometries ($\|^L$ and $\perp^r$). The most important prediction from the present work is the enhancement of the field-free (FF) $\bar{H}$ formation cross sections particularly at lower incident energies when the system (Ps+$\bar{p}$) is irradiated by a single mode, linearly polarized laser, the enhancement being more pronounced for a wider range of incident energy in the $\perp^r$ geometry than in the $\|^L$ one.

DOI: 10.1103/PhysRevA.74.022501 PACS number(s): 36.10.−k, 34.80.Qb

INTRODUCTION

One of the most important and promising mechanisms for the production of antihydrogen ($\bar{H}$) at low and intermediate energies is the three body charge transfer reaction in an orthopositronium (Ps)–antiproton ($\bar{p}$) system

$$\bar{p} + \mathrm{Ps}(nlm) \rightarrow \bar{\mathrm{H}}(n'l'm') + e. \qquad (1)$$

This reaction is particularly important because of its large cross sections leading to useful fluxes of $\bar{H}$ [1].

The production of a cold antihydrogen atom and the study of its properties and interactions offer a critical test of the fundamental symmetries in physics, particularly the *CPT* invariance [2–4] which is a fundamental property of quantum field theories in flat space-time resulting from the basic requirements of locality, Lorentz invariance and unitarity [5]. The experimental realization of the reaction (1) is supposed to provide slow and confined antihydrogen ($\bar{H}$) [6], necessary for the ultimate goal of high precision spectroscopic studies of $\bar{H}$. Although there is no experimental data for the process (1) available in the literature as yet, measurements were carried out by Merrison *et al.* [7] for the charge conjugate reaction, i.e., for the process $p+\mathrm{Ps}\rightarrow \mathrm{H}+e^+$ and the planning for the experimental setup for the process (1) is still in progress [1,8]. However quite a number of theoretical studies [9–22] were performed for the formation of antihydrogen in an antiproton-positronium charge transfer collision. In fact, a benchmark theoretical result exists in the literature on the reaction (1) due to Mitroy and his collaborators [14,15,17–19].

Since now-a-days in designing most of the collisional experiments, an external laser field is involved for different purposes (e.g., for cooling down the reaction constituents, confinement, collimation, etc.), it should be quite interesting and useful to study the collisional reaction [Eq. (1)] in the environment of an external laser field. In fact there exist a few theoretical works [23–30] in the literature on the production of antihydrogen (hydrogen) in the collision of an antiproton (proton) with positronium in the presence of the external laser [23–29] or magnetic fields [30]. One of the pioneering works along this line was due to Li *et al.* [23] where they studied the collision of the $\bar{p}$ with the ground state Ps to form the $\bar{H}$ (in the ground state) by using the first Born approximation (FBA) and obtained some enhancement in the total antihydrogen formation cross section when the system is irradiated by a laser field. Later, the same laser-assisted process (1) was also investigated by Whitehead *et al.* [27] and Voitkiv *et al.* [29] by using the classical trajectory Monte Carlo (CTMC) method and the FBA, respectively. The latter authors [29] studied the same process in the FBA at high incident energies (~100–1000 eV) using the circularly polarized laser field for both the post and the prior form of interactions. It should be pointed out here that in the calculation of Whitehead *et al.* [27], the authors treated $\bar{p}$ as the projectile and Ps as the stationary target, while in the present work (as also in the works of Li *et al.* [23,26] and Voitkiv *et al.* [29]) the reverse situation is considered. Thus the CTMC calculation [27] which deals with the heavy projectile $\bar{p}$ refers to the high collision energy range (~keV) while the other works [23,26,29], including the present one, refer to low and intermediate collision energy range (~eV), the projectile in these cases being the light particle Ps atom. From the experimental point of view, the above two approaches of theoretical calculations correspond to different experimental arrangements [1,6–9,12]. For the experimental realization of the present theoretical situation where the Ps is the projectile and the $\bar{p}$ is the stationary target, a cryogenic Penning trap could be used for the storage of the trapped cold antiproton (to be used as the target) while the projectile Ps formed by combining a positron to an electron (through charge transfer process) at the wall of the $\bar{p}$-ion trap [1,6–9,12] is allowed to interact with the trapped $\bar{p}$.

In view of the practical importance of the low energy antihydrogen formation in the environment of an external laser field, the need for some reliable theoretical estimates of the aforesaid reaction cross sections (particularly in the low collision energy regime) cannot be overemphasized, in the

absence of any experimental data. The previous quantum mechanical calculations [23,26,29] were performed using the FBA, which is basically meant for high incident energies. Further, for charge transfer reactions, the FBA is supposed to be inadequate, especially at high incident energies where higher order effects are supposed to contribute significantly. In fact, the need for the theoretical studies of the laser-assisted reaction (1) in an improved approximation beyond the FBA was already emphasized in earlier studies [27,29].

The present work attempts to fill this gap and addresses the same laser-assisted reaction (1) by resorting to an improved approximation, to be described below. In the present prescription, the collision dynamics is treated in the framework of the eikonal approximation, while the role of the external laser field is to modify the projectile (Ps) state, the final bound ($\bar{\mathrm{H}}$) state, as well as the continuum state of the ejected electron. The eikonal approximation [31,32], extensively applied for charge transfer reactions involving heavy projectiles, takes account of the higher order effects (with respect to the atomic interaction potential), which is essential for a rearrangement process especially at high incident energies (as mentioned above). Recently, the eikonal approximation was also successfully applied [31,33] to charge transfer problems involving light projectile, e.g., e^+-Ps even at quite low incident energies and a very good agreement was noted between the eikonal results [31] and the sophisticated close coupling results (using 22 states) of McAlinden *et al.* [34] for the Ps formation process at very low incident energies.

As for the laser-system interactions, the dressings of the target Ps and the $\bar{\mathrm{H}}$ atom (in the final channel) are considered perturbatively by solving the first order time dependent Schrödinger equation, while the interaction of the outgoing electron with the laser is treated nonperturbatively (to all orders) by choosing the appropriate Volkov wave function for it.

When the collisional system is irradiated by an external laser, some new degrees of freedom are introduced which, in turn, might influence the collision dynamics substantially depending upon the laser parameters, e.g., the intensity, the frequency, and the polarization direction of the laser field. The present calculations have been carried out for two polarization directions of the linearly polarized laser, e.g., parallel and perpendicular to the projectile momentum. In order to avoid the effect of the field ionization, the strength of the laser field is chosen to be much less than the atomic units of field strength (5×10^9 V/cm). Further, the frequency of the laser field is kept much below the binding energy of the Ps atom (6.8 eV).

THEORY

The present study deals with the following laser-assisted charge transfer process:

$$\bar{p} + \mathrm{Ps}(nlm) \pm \gamma(\omega,\vec{\varepsilon}) \rightarrow \bar{\mathrm{H}}(n'l'm') + e, \tag{2}$$

where $\gamma(\omega,\vec{\varepsilon})$ stands for the laser photon with frequency ω and field strength $\vec{\varepsilon}$. The laser field is treated classically and is chosen to be a single mode, linearly polarized, spatially homogeneous electric field represented by $\vec{\varepsilon}(t)=\vec{\varepsilon}_0 \sin \omega t$. The corresponding vector potential in the dipole approximation is $\vec{A}(t)=\vec{A}_0 \cos \omega t$ with $\vec{A}_0=\vec{\varepsilon}_0/\omega$. We use the atomic unit (a.u.) system throughout the work.

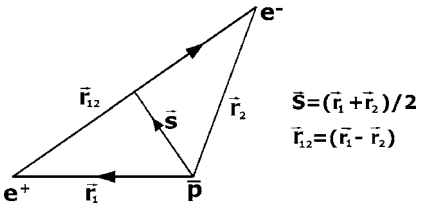

FIG. 1. Coordinate representation for the charge transfer process (1).

The coordinate system for the collision process is given in Fig. 1. $\vec{r}_1$ and $\vec{r}_2$ are the position vectors of the positron and the electron (e^+ and e^-), respectively, with respect to the target nucleus ($\bar{p}$) which is taken to be at rest at the origin.

The prior form of the transition matrix element for such laser-assisted charge transfer process is given by

$$T_{if} = -i\int_{-\infty}^{\infty} dt \langle \Psi_f^- | V_i | \psi_i \rangle, \tag{3}$$

where V_i is the perturbation potential in the initial channel,

$$V_i = \frac{1}{r_2} - \frac{1}{r_1}. \tag{4}$$

It is noted from Eq. (4) that the perturbation vanishes asymptotically.

The energy conservation relation for this process for the transfer of l photons is given by

$$E = \frac{k_i^2}{2\mu_i} + l\omega - \varepsilon_{\mathrm{Ps}} = \frac{k_f^2}{2} - \varepsilon_{\bar{\mathrm{H}}}, \quad l = 0, \pm 1, \pm 2, \cdots, \tag{5}$$

where "$+l$" refers to the absorption and "$-l$" refers to the emission of photons. In Eq. (5) $\vec{k}_i$ is the initial momentum of the Ps atom, $\vec{k}_f$ is the final momentum of the outgoing electron, μ_i is the reduced mass of the three body system in the initial channel, $\varepsilon_{\mathrm{Ps}}$ and $\varepsilon_{\bar{\mathrm{H}}}$ are the binding energies of the Ps and the $\bar{\mathrm{H}}$, respectively.

The initial channel asymptotic wave function ψ_i in Eq. (3) is given by

$$\psi_i = \chi_{k_i}(\vec{s},t)\phi_{\mathrm{Ps}}^d(\vec{r}_{12},t), \tag{6}$$

where $\chi_{k_i}(\vec{s},t)$ represents the incident plane wave for the Ps atom, normalized to a δ function

$$\chi_{k_i}(\vec{s},t) = (2\pi)^{-3/2} \exp[i(\vec{k}_i \cdot \vec{s} - E_i t)]. \tag{7}$$

It should be noted here that due to the symmetry of the charge, the phase term depending on the field parameters occurring in the plane wave Volkov solution for the e and e^+ constituting the Ps atom exactly cancels each other.

ϕ_{Ps}^{d}, representing the dressed wave function of the Ps atom in presence of the laser field is derived by solving the Schrödinger equation in the framework of first order time dependent perturbation theory using the Coulomb gauge and is given by (see Appendix)

$$\phi_{\mathrm{Ps}}^{d}=\frac{1}{\sqrt{8\pi}}e^{-iW_0^{\mathrm{Ps}}t}e^{-\lambda r_{12}}[1+i\vec{A}(t)\cdot\vec{r}_{12}], \tag{8}$$

where W_0^{Ps} is the unperturbed eigenenergy corresponding to the ground state of the Ps atom, $\lambda=1/2$ is the bound state parameter of the Ps. The laser-dressed bound state wave function of the $\bar{\mathrm{H}}$ in the final channel is also derived in a similar manner as in Eq. (8) to obtain

$$\phi_{\bar{\mathrm{H}}}^{d}=\frac{1}{\sqrt{\pi}}e^{-iW_0^{\bar{\mathrm{H}}}t}e^{-\alpha r_1}[1+i\vec{A}(t)\cdot\vec{r}_1], \quad \text{with } \alpha=1. \tag{9}$$

The effect of the laser field on the antiproton in the initial channel is neglected. This is quite legitimate on account of the heavy mass of the antiproton which is assumed to be the center (fixed) of the collision system.

The final channel exact wave function Ψ_f^- in Eq. (3) is approximated in the framework of the eikonal approximation and is chosen to be

$$\Psi_f^-=\chi_{k_f}(\vec{r}_2,t)\phi_{\bar{\mathrm{H}}}^{d}(\vec{r}_1,t). \tag{10}$$

$\chi_{k_f}(\vec{r}_2,t)$ in Eq. (10) denotes the dressed wave function (eikonal modified Volkov state) of the outgoing electron and is given by

$$\chi_{k_f}(\vec{r}_2,t)=(2\pi)^{-3/2}\exp[i(\vec{k}_f\cdot\vec{r}_2-\vec{k}_f\cdot\vec{\alpha}_0\sin\omega t - E_f t)]\exp\left[i\eta_f\int_z^{\infty}\left(\frac{1}{r_2}-\frac{1}{r_1}\right)dz'\right], \tag{11}$$

where the eikonal phase term (laser modified) accounts for the interaction (higher order effect) between the outgoing electron and the $\bar{\mathrm{H}}$ atom in the final channel with

$$\eta_f=\frac{1}{|\vec{k}_f-\vec{A}(t)|} \quad \text{and} \quad \vec{\alpha}_0=\frac{\vec{\epsilon}_0}{\omega^2}.$$

Performing the z' integration, Eq. (11) reduces to the following form:

$$\chi_{k_f}(\vec{r}_2,t)=(2\pi)^{-3/2}\exp[i(\vec{k}_f\cdot\vec{r}_2-\vec{k}_f\cdot\vec{\alpha}_0\sin\omega t-E_f t)]\times\left(\frac{r_2+r_{2z}}{r_{12}-r_{12z}}\right)^{i\eta_f}. \tag{12}$$

Now, in order to carry out the time integration in Eq. (3), we recast the eikonal modified Volkov state of the electron in the following manner [35]:

$$\chi_{k_f}(\vec{r}_2,t)=(2\pi)^{-3/2}\sum_{m=-\infty}^{\infty}(-i)^m J_m(\vec{k}_f\cdot\vec{\alpha}_0)\times\exp[i\{\vec{k}_f\cdot\vec{r}_2-(E_f-m\omega)t\}]\left(\frac{r_2+r_{2z}}{r_{12}-r_{12z}}\right)^{i\eta_f} \tag{12a}$$

In deducing Eq. (12a) we make use of the following generating function of the Bessel function [36]:

$$e^{ix\sin y}=\sum_{l=-\infty}^{\infty}J_l(x)e^{ily}. \tag{13}$$

After performing the time integration, the transition matrix element in Eq. (3) reduces to the following form [35,37]:

$$T_{if}=-\frac{i}{(2\pi)^2}\sum_l\delta(E_f-E_i-l\omega)I, \tag{14}$$

where "l" is the number of photons exchanged in the process. It should be noted that in performing the time integration analytically, we approximate the quantity $\vec{A}(t)$ in the eikonal phase term [Eq. (11)] by its $t=0$ value (A_0). The integral I in Eq. (14) is given by

$$I=\int\int d^3r_1\,d^3r_2\,e^{i\vec{k}_i\cdot\vec{r}_1}e^{i\vec{k}_f\cdot\vec{r}_2}\left(\frac{r_2+r_{2z}}{r_{12}-r_{12z}}\right)^{-i\eta_f}\phi_{\bar{\mathrm{H}}}^{d*}V_i\phi_{\mathrm{Ps}}^{d}J_l(\beta), \tag{15}$$

where $J_l(\beta)$ is the Bessel function of order l with

$$\beta=\vec{k}_f\cdot\vec{\alpha}_0. \tag{16}$$

The laser-assisted differential cross section for the formation of antihydrogen (with the transfer of l photons) is given as

$$\left(\frac{d\sigma}{d\Omega}\right)_l=\frac{\nu_f}{\nu_i}|T_{if}|^2, \tag{17}$$

where ν_f is the velocity of the ejected electron and ν_i is the velocity of the incident Ps atom.

Finally, the total laser-assisted differential cross section ($d\sigma/d\Omega$) for the $\bar{\mathrm{H}}$ formation is the sum over all multiphoton processes, i.e.,

$$\frac{d\sigma}{d\Omega}=\sum_{l=-\infty}^{\infty}\left(\frac{d\sigma}{d\Omega}\right)_l. \tag{18}$$

The total cross section (σ_l) for a given value of l is obtained by integrating the differential cross section in Eq. (17) over the solid angle, i.e.,

$$\sigma_l=\int\left(\frac{d\sigma}{d\Omega}\right)_l d\Omega, \tag{19}$$

while the total multiphoton cross section is given by

$$\sigma=\sum_{l=-\infty}^{\infty}\sigma_l. \tag{20}$$

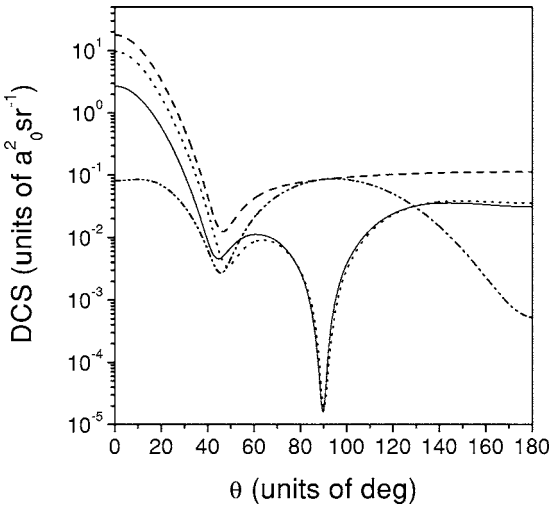

FIG. 2. Differential cross sections DCS (in units of $a_0^2\,\mathrm{sr}^{-1}$) vs scattering angle θ (in units of degree) for antihydrogen formation in the laser-assisted reaction $\bar{p}+\mathrm{Ps}(1s)\rightarrow\bar{\mathrm{H}}(1s)+e$ at an incident energy of the positronium $E_i=20$ eV, with a laser field strength $\varepsilon_0=1.5\times10^7$ V/cm, the photon energy $\hbar\omega=1.17$ eV, and for $\vec{\varepsilon}_0\|\vec{k}_i$. Solid curve: laser-assisted DCS for single photon absorption ($l=+1$); dotted curve: single photon emission ($l=+1$); dash dot dot curve: zero photon ($l=0$) transfer results; dashed curve represents the field-free (FF) differential cross section.

It should be noted that for the perpendicular polarization (i.e., when $\vec{\varepsilon}_0\perp\vec{k}_i$), the transition matrix element T_{if} in Eq. (3) is dependent on the azimuthal angle (φ) of the outgoing electron and as such for the perpendicular case we have performed the averaging over φ to obtain the corresponding differential as well as the total cross sections.

RESULTS AND DISCUSSIONS

We have computed the differential (DCS) as well as the total (TCS) cross sections for both the single photon ($l=\pm1$) and the multiphoton processes for the charge transfer reaction (2) using a linearly polarized, homogeneous, monochromatic laser field. The present study concerns the case when both the Ps and the $\bar{\mathrm{H}}$ atoms are in their ground ($1s$) states. The axis of quantization is chosen to be the direction of the external field $\vec{\varepsilon}_0$. We have calculated the cross sections for two directions of the laser polarization vector ($\vec{\varepsilon}_0$), e.g., $\vec{\varepsilon}_0$ is parallel to $\vec{k}_i$ ($\vec{\varepsilon}_0\|\vec{k}_i$) and $\vec{\varepsilon}_0$ is perpendicular to $\vec{k}_i$ ($\vec{\varepsilon}_0\perp\vec{k}_i$).

Figures 2 and 3 represent the DCS for the process (2) for no photon transfer ($l=0$, dash double dot curve), single photon absorption ($l=+1$, solid curve), and single photon emission ($l=-1$, dotted curve) processes at the incident Ps energy $E_i=20$ eV with the laser field strength $\varepsilon_0=1.5\times10^7$ V/cm and the laser frequency $\omega=1.17$ eV ($\lambda=1060$ nm) for $\vec{\varepsilon}_0\|\vec{k}_i$ and $\vec{\varepsilon}_0\perp\vec{k}_i$, respectively. The corresponding field-free (FF, dashed curve) results are also presented in Figs. 2 and 3 for comparison. The behavior of the single photon emission ($l=-1$) and absorption ($l=+1$) DCS is more or less similar,

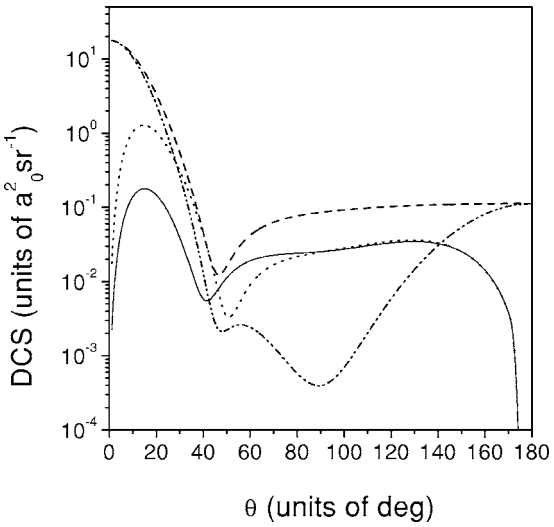

FIG. 3. Same as Fig. 2, but for $\vec{\varepsilon}_0\perp\vec{k}_i$.

except for some quantitative difference at forward scattering angles, the emission DCS being always higher than the absorption one for both the geometries ($\|^L$ and $\perp^r$). For the parallel geometry (vide Fig. 2), the $l=\pm1$ curves exhibit a deep minimum exactly at 90°, while in contrast, the $l=0$ curve shows a broad maximum around 90°. The above behavior could be explained as follows. Since for $\vec{\varepsilon}_0\|\vec{k}_i$, the argument $\beta=\vec{k}_f\cdot\vec{\alpha}_0$ of the Bessel function $J_l(\beta)$ in Eq. (15) becomes zero for the scattering angle $\theta=90°$, the transition matrix element vanishes at that particular angle, as $J_{\pm1}(\beta)$ is zero for $\beta=0$. On the contrary, for $l=0$ case, since $J_0(0)$ is unity, the DCS curve in Fig. 2 shows a broad maximum around 90°.

For the perpendicular geometry (see Fig. 3), on the other hand, due to the same reasons, the DCS curves for $l=\pm1$

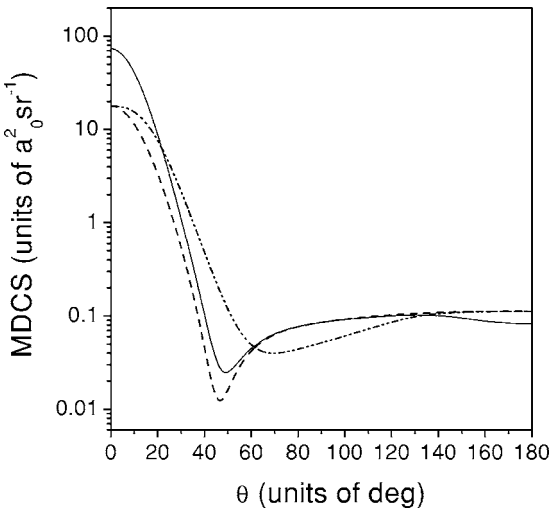

FIG. 4. Multiphoton differential cross sections MDCS (in units of $a_0^2\,\mathrm{sr}^{-1}$) vs scattering angle θ (in units of degree) at $E_i=20$ eV, with the laser field strength $\varepsilon_0=5.14\times10^7$ V/cm and the photon energy $\hbar\omega=1.17$ eV. Solid curve: MDCS for the parallel ($\|^L$) geometry; dash dot dot curve: MDCS for the perpendicular ($\perp^r$) geometry, dashed curve: FF results.

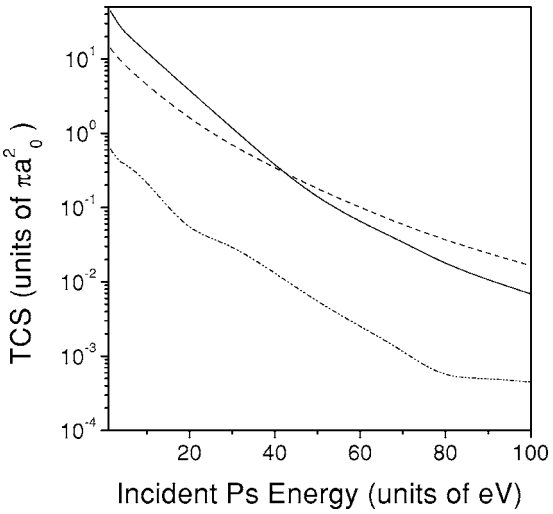

FIG. 5. Total cross section TCS (in units of πa_0^2) vs the incident Ps energy (in units of eV) distribution for the $\|^L$ geometry, the laser parameters are remaining the same as in Fig. 4. Solid curve: multiphoton total cross section (MTCS), summed over the photon number l; dotted curve: single photon absorption TCS, dash dot dot curve: FF TCS.

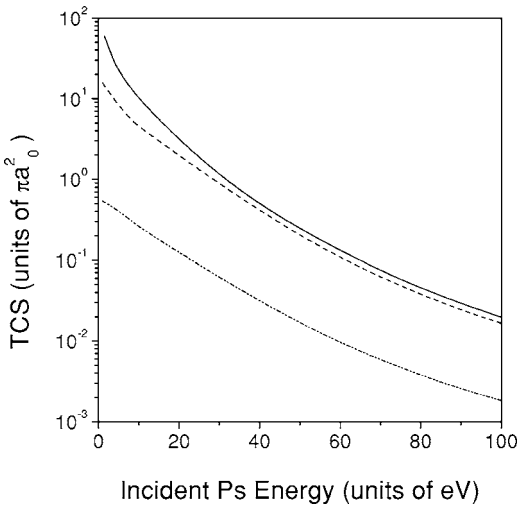

FIG. 6. Same as Fig. 5, but for the $\perp^r$ geometry.

vanish at $\theta=0°$ and 180° (since for $\vec{\varepsilon}_0 \perp \vec{k}_i$, the argument of J_l is $-k_f \alpha_0 \sin\theta \cos\varphi$), while for $l=0$, a deep minimum is noted at $\theta=90°$.

Figure 4 exhibits the angular variation of the multiphoton differential cross sections (MDCS) for both the geometries with $\varepsilon_0=5.14\times10^7$ V/cm, $\omega=1.17$ eV, and the incident Ps energy $E_i=20$ eV. As may be revealed from the figure, the $\bar{H}$ production is enhanced in the presence of the background laser field, particularly in the forward directions ($\sim0°-60°$) irrespective of the geometry. This behavior may be contrasted with that of the FBA results due to Li *et al.* [26], where they obtained the enhancement in the aforesaid ($\sim0°-60°$) angular range for the perpendicular geometry only, while for the parallel geometry, the laser-assisted $\bar{H}$ production cross sections were found [26] to be suppressed as compared to the FF ones, particularly at lower scattering angles ($\sim0°-20°$). As for the quantitative comparison, the magnitude of the enhancement is found to be larger in the present eikonal approximation than in the FBA due to Li *et al.* [26] for both the geometries.

Figures 5 and 6 depict the multiphoton total cross sections (MTCS) for the $\bar{H}$ formation versus the incident Ps energy for the parallel and the perpendicular geometry, respectively, with $\varepsilon_0=5.14\times10^7$ V/cm and $\omega=1.17$ eV. The MTCS, summed over l ($\Sigma_{l=-\infty}^{\infty}\sigma_l$) as well as the TCS for the single photon absorption ($l=+1$) are represented in both the figures 5 and 6 along with the FF results. As may be noted from Fig. 5, for $\vec{\varepsilon}_0 \| \vec{k}_i$, the multiphoton total cross sections ($\Sigma_{l=-\infty}^{\infty}\sigma_l$, solid curve) are enhanced by the irradiation of the laser at low and intermediate energies ($\sim$0–45 eV), while at higher incident energies, the situation is just the reversed, i.e., the MTCS is suppressed as compared to the FF one. For the perpendicular geometry (Fig. 6), on the other hand, the

TABLE I. Laser-assisted $\bar{H}$ formation cross sections (for $l=\pm1$ as well as for multiphoton transfers) at different incident Ps energies along with the field-free TCS using a linearly polarized laser field with a field strength $\varepsilon_0=5.14\times10^7$ V/cm and the photon energy $\hbar\omega=1.17$ eV. The numbers in square brackets denote the powers of ten.

	Laser assisted $\bar{H}$ formation cross sections						
	$\|^L$ geometry			$\perp^r$ geometry			
Incident Ps energy (eV)	Emission $l=-1$ TCS	Absorption $l=+1$ TCS	Multiphoton $\Sigma_l\sigma_l$ TCS	Emission $l=-1$ TCS	Absorption $l=+1$ TCS	Multiphoton $\Sigma_l\sigma_l$ TCS	Field free TCS
1.5	7.80	0.61	43.97	10.63	0.52	59.16	13.79
3.5	1.06	0.41	28.15	6.83	0.44	31.24	9.95
50	0.0057	0.005	0.12	0.058	0.015	0.23	0.17
100	0.0008	0.0006	0.0006	0.0044	0.0017	0.019	0.016
200	2.46[−5]	2.15[−5]	0.005	0.00024	0.0004	0.0009	0.00084
300	1.53[−6]	1.22[−6]	2.44[−5]	2.70[−5]	1.82[−5]	0.00012	0.00012
400	7.97[−7]	2.02[−7]	4.61[−6]	3.22[−6]	2.34[−6]	2.74[−5]	2.84[−5]
500	7.77[−8]	8.08[−8]	1.26[−6]	4.57[−7]	3.53[−7]	8.22[−6]	8.92[−6]

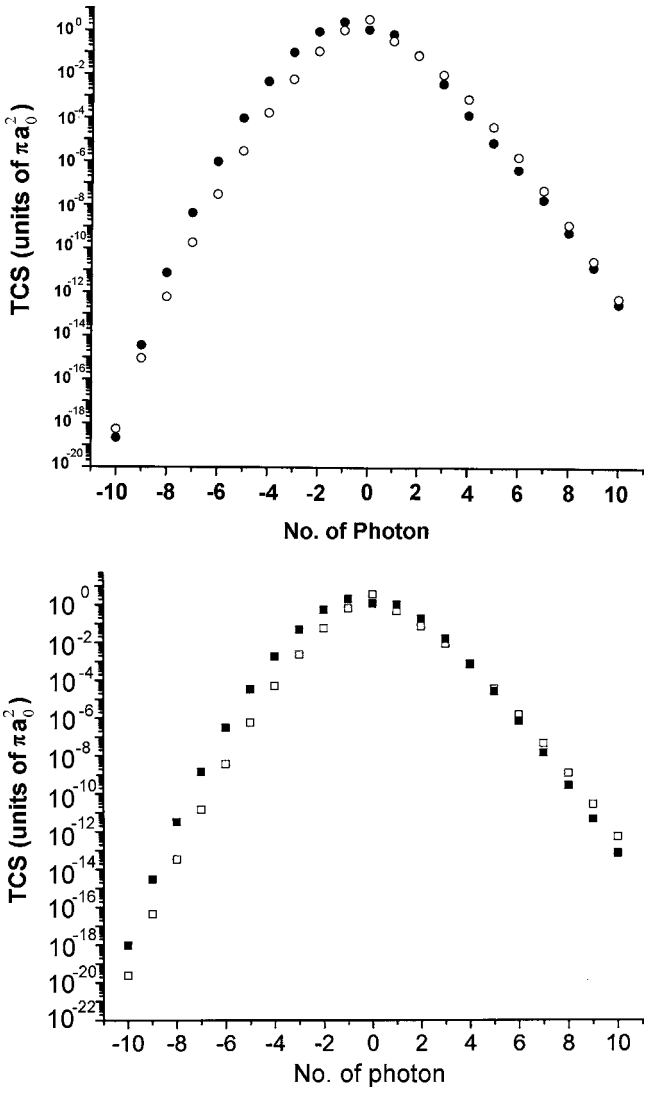

FIG. 7. (a) TCS (in units of πa_0^2) vs the number of photon at an incident energy for $E_i=10$ eV, with laser field strength $\varepsilon_0=1.5\times10^7$ V/cm and photon energy $\hbar\omega=1.17$ eV; filled circles: results for $\vec{\varepsilon}_0\|\vec{k}_i$; open circles: results for $\vec{\varepsilon}_0\perp\vec{k}_i$. (b) Same as (a), but without the atomic dressing terms (both for Ps and $\bar{\mathrm{H}}$). Filled squares: results for $\vec{\varepsilon}_0\|\vec{k}_i$; open squares: results for $\vec{\varepsilon}_0\perp\vec{k}_i$.

MTCS ($\Sigma_{l=-\infty}^{\infty}\sigma_l$) is always enhanced, though the enhancement decreases with increasing incident energy. However, for the single photon absorption, the TCS is ($\sim$0–100 eV) significantly suppressed irrespective of the geometry (vide Figs. 5 and 6) indicating the importance of the higher l contributions to the $\bar{\mathrm{H}}$ formation cross section.

Table I gives a numerical measure of the single photon ($l=\pm1$) as well as the multiphoton total cross sections (MTCS) for both the geometries ($\|^L$ and $\perp^r$) for a wide range of the incident Ps energy ($\sim$1.5–500 eV). Comparison between the two geometries indicates that the cross sections (both the single photon as well as the MTCS) are quite sensitive with respect to the geometries. Table I also reflects that at low and intermediate incident energies, the MTCS are significantly enhanced with respect to the field-free TCS, while in contrast, at higher incident energies the laser-assisted cross sections are found to be suppressed. It is further revealed from Table I that at low incident energies, the enhancement in the MTCS is highly pronounced for the $\perp^r$ geometry than in the $\|^L$ one. This could probably be attributed [26] to the effect of the polarization of the electron and the positron cloud of the Ps in the laser field, i.e., stretching of the Ps atom along the direction of the polarization, while shrinkage along the $\perp^r$ direction.

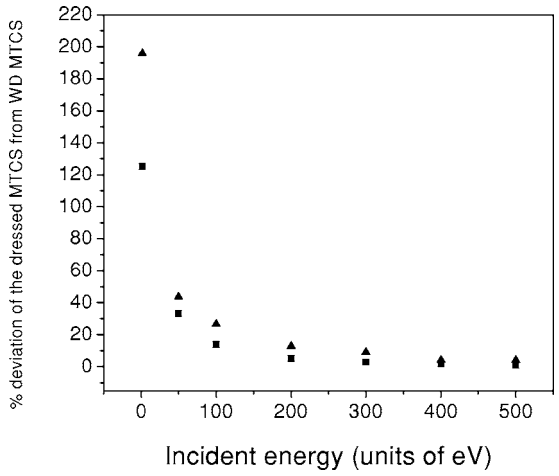

FIG. 8. Percentage (%) deviation of the dressed MTCS from without dressing (WD) MTCS with respect to the incident Ps energy (in units of eV) for both the geometries. Filled squares: results for parallel geometry; filled triangles: results for perpendicular geometry.

Figure 7(a) displays the distribution of the total cross sections (TCS) among the multiphoton processes. It is revealed from the figure that for a given value of l the photon emission process ($l<0$) in the parallel geometry dominates over the perpendicular geometry, while for the absorption ($l>0$) process the perpendicular geometry is favored. Figure 7(b) depicts the same distribution as in Fig. 7(a) but without the atomic dressing terms (both Ps and $\bar{\mathrm{H}}$). Comparing the two figures [7(a) and 7(b)] it may be inferred that for the absorption case ($l>0$), the atomic dressing terms play a major role in enhancing the $\bar{\mathrm{H}}$ formation cross section (TCS) in the $\perp^r$ geometry than in the $\|^L$ one, particularly for the lower values of l. For the emission case, on the other hand, the atomic dressing is found [vide Figs. 7(a) and 7(b)] to enhance without dressing (WD) cross sections, irrespective of the geometry.

Figure 8 reflects the effect of the atomic dressings (Ps and $\bar{\mathrm{H}}$) with respect to the incident Ps energy for both the parallel and perpendicular geometries. It is noted from the figure that due to the presence of the atomic dressing, the multiphoton total cross sections (MTCS) are enhanced with respect to the corresponding WD results and the difference between the two (dressed MTCS and WD MTCS) dies down with increasing incident energy for both the geometries. Figure 8 further reveals that the atomic dressing effect is more pronounced in the perpendicular geometry than in the parallel one, particularly at low and intermediate incident energies.

We now present in Fig. 9 the variation of the multiphoton TCS (MTCS) with respect to the laser photon energy ($h\nu$,

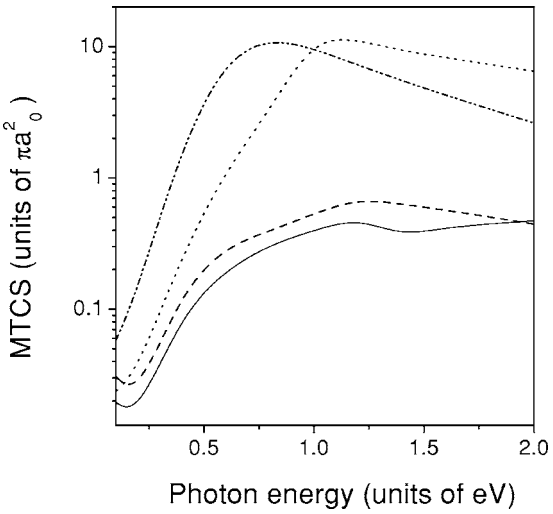

FIG. 9. MTCS (in units of πa_0^2) vs laser photon energy (in units of eV) for E_i=10 eV, laser parameters are remaining the same as in Fig. 4. Solid curve: absorption MTCS for the $\|^L$ geometry; dashed curve: absorption MTCS for the $\perp^r$ geometry; dotted curve: emission MTCS for the $\|^L$ geometry; dash dot dot curve: emission MTCS for the $\perp^r$ geometry.

$\sim$0–2 eV) for the individual absorption and the emission processes with the laser field strength $\varepsilon_0=5.14\times10^7$ V/cm at the incident Ps energy 10 eV for both the geometries. As may be revealed from the figure, for this particular charge transfer reaction (2), the photon emission process is very dominant over the absorption one (irrespective of the geometry), as is expected for an exothermic reaction 2. As regards the geometry, it may be noted (from Fig. 9) that although the qualitative behavior of the emission/absorption MTCS is more or less similar for the two geometries, the quantitative difference between them (the two geometries) is quite significant particularly for the photon emission process.

Figure 10 exhibits the variation of the MTCS against the laser field strength ε_0 in atomic unit (in units of 5.14×10^9 V/cm). As may be revealed from the figure, the

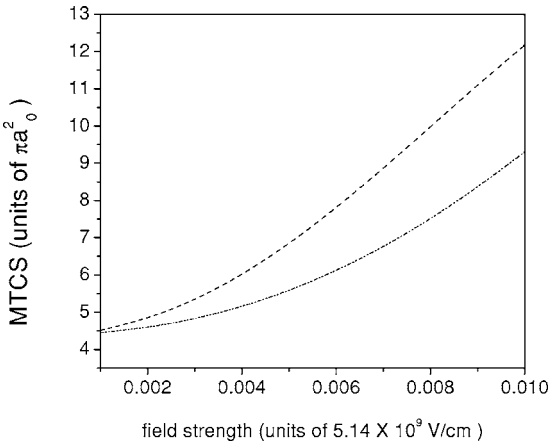

FIG. 10. MTCS (in units of πa_0^2) vs laser field strength (in units of 5.14×10^9 V/cm), other parameters are the same as in Fig. 9. Dashed curve: MTCS results for the $\|^L$ geometry; dash dot dot curve: MTCS results for the $\perp^r$ geometry.

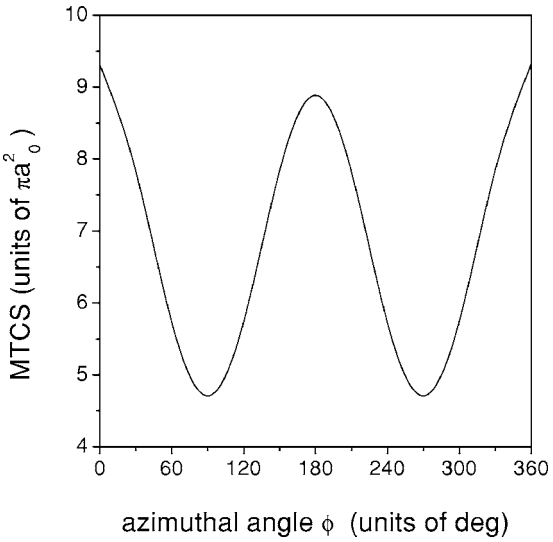

FIG. 11. Variations of the MTCS with respect to the azimuthal angles (for $\perp^r$ geometry). Other parameters are the same as in Fig. 9.

MTCS increases nonlinearly with respect to ε_0 for both the geometries ($\vec{\varepsilon}_0\|\vec{k}_i$ and $\vec{\varepsilon}_0\perp\vec{k}_i$), although the rate of enhancement is much higher for the parallel geometry than that for the perpendicular one.

Figure 11 describes the dependence of the multiphoton TCS on the azimuthal angle φ for the perpendicular geometry (the $\|^L$ geometry being independent of φ). As is noted from the figure, the MTCS having a periodic variation with respect to φ exhibits maxima at φ=0°, 180° and minima at 90° and 270°. Similar qualitative behavior of the φ dependence was also noted by Li *et al.* [26] in their FBA results at the differential cross section level. The above features of the MTCS against φ could be explained physically [26] as well as mathematically in view of the properties of the Bessel functions as follows. For the perpendicular geometry the argument of the Bessel function that depends both on θ and φ (unlike the parallel case) assumes the value $-k_f \sin\theta\cos\varphi$. Thus for φ=90° and 270°, the values of the Bessel functions for all orders (except for J_0) become zero [since $J_l(0)=0$ for nonzero values of l] and as such the contribution to the MTCS from all l values (except for l=0) vanishes at φ=90° and 270°. On the other hand, for φ=0° and 180°, the argument of the Bessel function attains its maximum value and hence the MTCS exhibits maxima at those azimuthal angles, the scattering angle θ being integrated out in the TCS.

With a view to optimizing the laser field effect we have computed the multiphoton total $\bar{H}$ formation cross sections (MTCS) for a wide range of experimentally realizable [38–47], as well as theoretically feasible (within the limitation of the model), laser parameters. Further, it should be pointed out here that the frequency of the laser field should be kept much below the Ps breakup threshold (6.8 eV). The detailed results are tabulated in Table II which reveals the following salient features. The maximum enhancement in the $\bar{H}$ formation cross sections at low incident energies is obtained for the laser parameters, ε_0=0.1 a.u., ω=0.074 a.u.,

TABLE II. Laser-assisted $\bar{H}$ formation cross sections (MTCS) for different laser field strengths and frequencies along with the field free TCS results. The numbers is square brackets denote the powers of ten.

Field Strength (a.u.)	Incident Ps energy (eV)	Field-free TCS (a.u.)	MTCS results for $\|^L$ geometry (a.u.)			MTCS results for $\perp^r$ geometry (a.u.)		
			Frequency =1.17 eV	Frequency =2.0 eV	Frequency =3.406 eV	Frequency =1.17 eV	Frequency =2.0 eV	Frequency =3.406 eV
0.01	10	1.37	12.18	7.59	—	9.31	6.08	—
	15	7.99[−01]	7.19	4.43	3.25	4.76	3.31	2.85
	20	4.92[−01]	4.18	2.74	2.00	2.69	1.96	1.72
	25	3.17[−01]	2.29	1.77	1.28	1.62	1.22	1.09
	30	2.11[−01]	1.16	1.18	8.53[−01]	1.03	8.00[−01]	7.20[−01]
	40	1.02[−01]	2.84[−01]	5.69[−01]	4.11[−01]	4.64[−01]	3.77[−01]	3.44[−01]
	50	5.42[−02]	1.17[−01]	2.98[−01]	2.16[−01]	2.33[−01]	1.96[−01]	1.81[−01]
	80	1.15[−02]	1.67[−02]	6.03[−02]	4.47[−02]	4.48[−02]	4.00[−02]	3.78[−02]
	100	5.00[−03]	6.64[−03]	2.52[−02]	1.91[−02]	1.87[−02]	1.72[−02]	1.64[−02]
	150	9.50[−04]	9.12[−04]	4.21[−03]	3.51[−03]	3.32[−03]	3.18[−03]	3.08[−03]
	200	2.63[−04]	1.97[−04]	9.66[−04]	9.48[−04]	8.84[−04]	8.68[−04]	8.50[−04]
	250	9.23[−05]	6.04[−05]	2.60[−04]	3.26[−04]	3.00[−04]	3.00[−04]	2.97[−04]
	300	3.80[−05]	2.44[−05]	7.94[−05]	1.33[−04]	1.21[−04]	1.22[−04]	1.22[−04]
	400	8.95[−06]	4.61[−06]	1.30[−05]	3.06[−05]	2.74[−05]	2.84[−05]	2.86[−05]
	500	4.87[−06]	1.26[−06]	4.17[−06]	9.47[−06]	8.22[−06]	8.86[−06]	8.98[−06]
0.02	10		6.22	13.59	-	20.68	11.47	—
	15		2.81	8.50	5.08	10.56	5.79	3.76
	20		1.28	5.59	3.18	5.73	3.24	2.18
	25		6.65[−01]	3.79	2.07	3.30	1.94	1.34
	30		4.26[−01]	2.62	1.39	2.00	1.22	8.70[−01]
	40		1.55[−01]	1.27	6.77[−01]	8.24[−01]	5.45[−01]	4.03[−01]
	50		5.70[−02]	6.03[−01]	3.56[−01]	3.82[−01]	2.70[−01]	2.07[−01]
	80		9.12[−03]	5.02[−02]	7.15[−02]	6.12[−02]	5.03[−02]	4.17[−02]
	100		3.34[−03]	1.16[−02]	2.98[−02]	2.36[−02]	2.07[−02]	1.77[−02]
	150		4.64[−04]	1.88[−03]	5.11[−03]	3.33[−03]	3.61[−03]	3.26[−03]
	200		1.07[−04]	3.18[−04]	1.30[−03]	7.69[−04]	9.50[−04]	8.88[−04]
	250		3.09[−05]	1.09[−04]	4.23[−04]	2.61[−04]	3.22[−04]	3.07[−04]
	300		1.20[−05]	3.37[−04]	1.61[−04]	1.06[−04]	1.30[−04]	1.26[−04]
	400		2.33[−06]	6.88[−06]	3.16[−05]	2.28[−05]	2.95[−05]	2.91[−05]
	500		6.53[−07]	2.05[−06]	7.76[−06]	6.78[−06]	9.07[−06]	9.06[−06]
0.1	10		2.23	11.66	—	32.10	197.72	—
	15		7.35[−01]	4.02	8.43	17.41	100.83	43.00
	20		2.69[−01]	2.47	6.44	9.28	50.39	23.75
	25		1.24[−01]	1.22	4.61	4.66	26.01	13.83
	30		6.55[−02]	5.25[−01]	3.37	2.15	13.99	8.40
	40		2.02[−02]	2.42[−01]	1.82	3.27[−01]	4.88	3.42
	50		3.92[−03]	7.77[−02]	6.41[−01]	6.85[−02]	1.88	1.54
	80		1.56[−04]	8.36[−03]	5.57[−02]	8.81[−04]	1.38[−01]	2.22[−01]
	100		2.82[−04]	3.13[−03]	2.02[−02]	2.31[−03]	5.53[−02]	7.88[−02]
	150		6.98[−05]	3.39[−04]	1.39[−03]	5.06[−04]	7.38[−03]	1.03[−02]
	200		1.75[−05]	7.37[−05]	2.54[−04]	1.09[−04]	1.55[−03]	2.19[−03]
	250		5.81[−06]	2.20[−05]	7.09[−05]	3.74[−05]	3.57[−04]	6.33[−04]
	300		2.08[−06]	8.06[−06]	2.65[−05]	1.54[−05]	9.71[−05]	2.25[−04]
	400		4.09[−07]	1.64[−06]	4.56[−06]	2.96[−06]	1.25[−05]	4.08[−05]
	500		1.16[−07]	4.21[−07]	1.29[−06]	8.13[−07]	3.82[−06]	1.05[−05]

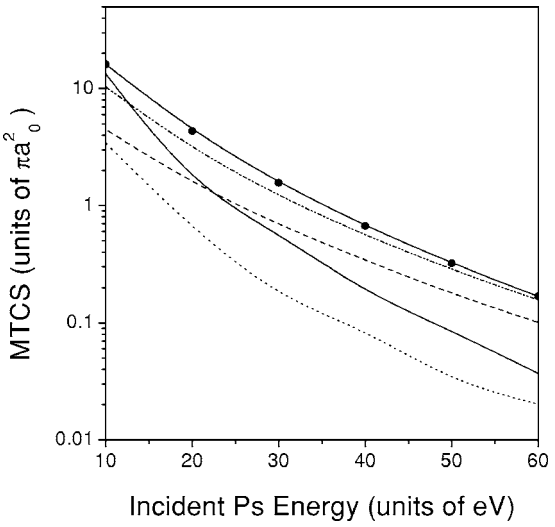

FIG. 12. MTCS vs the incident Ps energy to compare the FBA and the present eikonal results with laser field strength $\varepsilon_0=8.0\times10^7$ V/cm and photon energy $\hbar\omega=1.17$ eV. Solid curve: present eikonal results for the $\|^L$ geometry; dotted curve: FBA results for the $\|^L$ geometry; solid curve with solid circles: present eikonal result for $\perp^r$ geometry; dash dot dot curve: FBA results for the $\perp^r$ geometry; dashed curve: FF results.

and when the laser polarization is $\perp^r$ to the incident Ps momentum. For the parallel polarization, on the other hand, the enhancement is found to be maximum (though less than that of the $\perp^r$ case) for a lower laser field strength (e.g., $\varepsilon_0=0.02$ a.u.) with the same frequency $\omega=0.074$ a.u. At higher incident energies, the enhancement is noted for higher values of ω (e.g., $\omega=0.125$ a.u.) for a given field strength (ε_0) for both the geometries. It should be pointed out here that in Table II, only those results are quoted for which enhancement (in the MTCS) is obtained.

In what follows, we compare the present eikonal results with the existing theoretical results [26,29]. Figure 12 represents a comparative study between the first Born approximation (FBA) and the present eikonal approximation for both the parallel and the perpendicular geometries. It is evident from Fig. 12 that at low and intemediate incident energies (~1–60 eV), the present eikonal MTCS are always higher than the corresponding FBA [26] ones (for both the geometries), indicating the need for higher order approximation beyond the FBA.

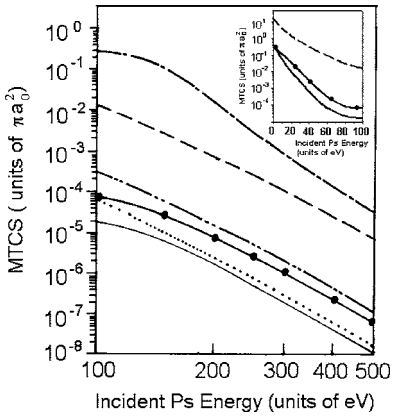

FIG. 13. Same as in Fig. 12, but for the higher incident energies (incident Ps energies are given in log scale) with laser field strength $\varepsilon_0=5.14\times10^7$ V/cm and photon energy $\hbar\omega=0.117$ eV; dash dot curve: FBA result using a circularly polarized laser field (Voitkiv *et al.* [29]). Inset: low energy laser-assisted eikonal results (both $\|^L$ and $\perp^r$ geometries) along with the field-free TCS (laser parameters remain same).

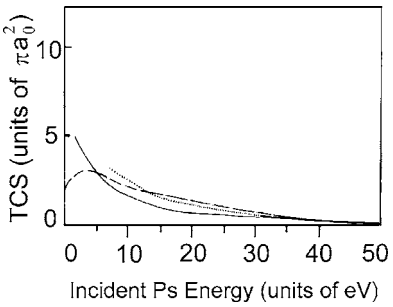

FIG. 14. Comparative study of the present eikonal TCS (field free) with the close coupling results of Mitroy and his collaborators [14,18] at low incident energies (~0–50 eV). Solid curve: present FF eikonal results; dashed curve: close coupling results due to Mitroy and Stelbovics [14]; dotted curve: more accurate close coupling results due to Mitroy and Ryzhikh [18].

In Fig. 13 we have compared the present $\bar{H}$ formation MTCS with another existing FBA results by Voitkiv *et al.* [29] using a circularly polarized laser field with a low laser frequency ($\omega=0.0043$ a.u.) at higher incident energies (e.g., ~100–1000 eV). It is evident from Fig. 13 that at this low frequency, the present eikonal MTCS (with linear polarization) are suppressed with respect to the FF ones, irrespective of the incident energy (vide the inset of Fig. 13), in contrast to the FBA results [29] (with circular polarization), which are found to enhance slightly. However, it should be pointed out here (as already mentioned before) that for the charge transfer reaction a higher order approximation (beyond FBA) is essential for a reliable estimate of the cross sections particularly at high incident energies.

Finally, in order to justify the present eikonal results at low incident energies (~5–50 eV), we have compared our field-free TCS with the close coupling (CC) results of Mitroy and his collaborators [14,18] in Fig. 14. As is evident from the figure, the present eikonal results agree reasonably well, particularly with the authors' most accurate CC results [18] (the dotted curve in Fig. 14) for the incident energies 5 eV onwards. This agreement extends a good support to our low energy results (~5–50 eV) for the laser-assisted $\bar{H}$ formation in the framework of the eikonal approximation. However, it is apparent from Fig. 14 that below 5 eV the present results diverge from those of the more elaborate treatments [14].

CONCLUSIONS

The following inferences could be drawn from the present studies:

(1) With the proper choice of the laser parameters, the multiphoton total $\bar{H}$ formation cross sections (MTCS) are enhanced in presence of a background laser field. The MTCS is quite sensitive with respect to the field polarization direction, e.g., the perpendicular geometry is more favored for the formation of antihydrogen than the parallel geometry. Further, for the perpendicular geometry, enhancement is maintained for a wider incident energy range (with respect to the field free cross sections) than for the parallel one.

(2) The effect of the atomic dressing (particularly for the Ps atom) is more prominent in the perpendicular geometry than in the parallel geometry.

(3) In the case of photon emission ($l<0$) the $\|^L$ geometry is favored for the $\bar{H}$ formation, while for the absorption ($l>0$), the reverse is true, i.e., the $\perp^r$ geometry is preferred.

(4) The photon emission process ($l<0$) is very dominant over the absorption one ($l>0$), particularly at lower incident energies, as is expected for an exothermic reaction (2).

(5) The laser-assisted $\bar{H}$ formation cross section is supposed to be further enhanced if the Ps can be prepared in a highly excited state [6,8,12].

Lastly, it may be inferred from the present theory that (to be verified by the future experiment) for greater enhancement of the $\bar{H}$ formation cross section (MTCS) through the reaction (2), the laser polarization (for a linearly polarized laser) along the perpendicular direction of the incident momentum could be suggested.

APPENDIX

In order to find the dressed wave function for the Ps ($\bar{H}$) atom in the initial (final) channel in the framework of the first order perturbation theory [48], we solve the following inhomogeneous differential equation

$$\left(-\frac{\hbar^2}{2m}\nabla^2 - \frac{q^2}{r} - E_0\right)\psi_1 = -H'\psi_0, \tag{A1}$$

q being the charge of the particle and $E_0 = -\frac{q^2}{2a_0}$.

In Eq. (A1) H' is the perturbation given by $H' = i\frac{\hbar}{m}q\vec{A}\cdot\vec{\nabla}$ in the Coulomb gauge, ψ_1 is the perturbed wave function, and ψ_0 is the unperturbed wave function for the Ps ($\bar{H}$) atom, given by

$$\psi_0 = C_1 e^{-\lambda r},$$

where C_1 is the normalization constant for the bound state.

To solve Eq. (A1) we first choose the trial solution as

$$\psi_1(\vec{r}) = f(r)\cos\theta. \tag{A2}$$

Substituting ψ_1 and using the expression of ∇^2 in the spherical polar coordinate in Eq. (A1) we obtain

$$\frac{d^2f}{dr^2} + \frac{2}{r}\frac{df}{dr} - \frac{2}{r^2}f + \frac{2\lambda}{r}f - \lambda^2 f = -2iq\lambda C_1 A e^{-\lambda r}. \tag{A3}$$

Now, in order to solve the above inhomogeneous differential equation (A3) by the power series method, we choose

$$f = e^{-\lambda r}\sum_{n=0}^{\infty} b_n r^n. \tag{A4}$$

Substituting the values of f, $\frac{df}{dr}$, and $\frac{d^2f}{dr^2}$ in Eq. (A3) and equating the coefficients of equal power of r from both sides of Eq. (A3), we obtain

$$b_1 = iqC_1A, \quad b_2 = b_3 = b_4 = \cdots = 0.$$

Hence the radial part of the perturbed wave function (ψ_1) in Eq. (A2) becomes

$$f = (b_0 + iqAC_1 r)e^{-\lambda r}. \tag{A5}$$

Now from the boundary condition we have $f \to 0$, when $A \to 0$.Hence, $b_0=0$ in Eq. (A5), which leads to

$$f = iqAC_1 re^{-\lambda r}. \tag{A6}$$

Thus in view of Eqs. (A2), (A6), and (A7), the solution ψ_1 is obtained as

$$\psi_1 = iqC_1(\vec{A}\cdot\vec{r})e^{-\lambda r}. \tag{A7}$$

Hence the total dressed wave function becomes

$$\psi_d = (1 + iq\vec{A}\cdot\vec{r})\psi_0 = (1 + iq\vec{A}\cdot\vec{r})C_1 e^{-\lambda r}. \tag{A8}$$

Similar wave function for the ground state of the Ps ($\bar{H}$) was derived by Li *et al.* [23,26] through a different approach.

[1] B. I. Deutch, L. H. Andersen, P. Hvelplund, F. M. Jacobsen, H. Knudsen, M. H. Holzscheiter, M. Charlton, and G. Laricchia, Hyperfine Interact. **44**, 271 (1988).

[2] G. Gabrielse, N. S. Bowden, P. Oxley, A. Speck, C. H. Storry, J. N. Tan, M. Wessels, D. Grzonka, W. Oelert, G. Schepers, T. Sefzick, J. Walz, H. Pittner, T. W. Hänsch, and E. A. Hessels, Phys. Rev. Lett. **89**, 213401 (2002).

[3] G. Gabrielse, N. S. Bowden, P. Oxley, A. Speck, C. H. Storry, J. N. Tan, M. Wessels, D. Grzonka, W. Oelert, G. Schepers, T. Sefzick, J. Walz, H. Pittner, T. W. Häsch, and E. A. Hessels, Phys. Rev. Lett. **89**, 233401 (2002).

[4] M. Amoretti *et al.*, Nature (London) **419**, 456 (2002).

[5] M. H. Holzscheiter and M. Charlton, Rep. Prog. Phys. **62**, 1 (1999).

[6] M. Charlton, J. Eades, D. Horvath, R. J. Hughes, and C. Zimmermann, Phys. Rep. **241**, 65 (1994).

[7] J. P. Merrison, H. Bluhme, J. Chevallier, B. I. Deutch, P. Hvelplund, L. V. Jørgensen, H. Knudsen, M. R. Poulsen, and M. Charlton, Phys. Rev. Lett. **78**, 2728 (1997).

[8] B. I. Deutch, M. Charlton, M. H. Holzscheiter, P. Hvelplund, L. V. Jørgensen, H. Knudsen, G. Laricchia, J. P. Merrison, and M. R. Poulsen, Hyperfine Interact. **76**, 155 (1993).

[9] J. W. Humberston, M. Charlton, F. M. Jacobson, and B. I. Deutch, J. Phys. B **20**, L25 (1987).

[10] J. W. Darewych, J. Phys. B **20**, 5917 (1987).
[11] S. N. Nahar and J. M. Wadehra, Phys. Rev. A **37**, 4118 (1988).
[12] M. Charlton, Phys. Lett. A **143**, 143 (1990).
[13] S. Tripathi, C. Sinha, and N. C. Sil, Phys. Rev. A **32**, 1785 (1990).
[14] J. Mitroy and A. T. Stelbovics, Phys. Rev. Lett. **72**, 3495 (1994).
[15] J. Mitroy and A. T. Stelbovics, J. Phys. B **27**, L79 (1994).
[16] S. Tripathi, R. Biswas, and C. Sinha, Phys. Rev. A **51**, 3584 (1995).
[17] J. Mitroy, Phys. Rev. A **52**, 2859 (1995).
[18] J. Mitroy and G. Ryzhikh, J. Phys. B **30**, L371 (1997).
[19] D. B. Cassidy, J. P. Merrison, M. Charlton, J. Mitroy, and G. Ryzhikh, J. Phys. B **32**, 1923 (1999).
[20] C. Y. Hu, D. Caballero, and Z. Hlousek, J. Phys. B **34**, 331 (2001).
[21] J. S. Briggs and E. A. Solov'ev, J. Phys. B **34**, 1337 (2001).
[22] N. Yamanaka and Y. Kino, Phys. Rev. A **65**, 062709 (2002).
[23] S. M. Li, Z. J. Chen, Z. F. Zhou, and Q. Q. Wang, Phys. Rev. A **59**, 1697 (1999).
[24] L. B. Madsen and P. Lambropoulos, Phys. Rev. A **61**, 067401 (2000).
[25] B. Malakar, A. Bandyopadhyay, and M. Bhattacharya, Phys. Scr. **61**, 657 (2000).
[26] S. M. Li, A. H. Liu, Z. F. Zhou, and J. Chen, J. Phys. B **33**, 4627 (2000).
[27] R. J. Whitehead, J. F. McCann, and I. Shimamura, Phys. Rev. A **64**, 023401 (2001).
[28] J. S. Cohen, Phys. Rev. A **67**, 017401 (2003).
[29] A. B. Voitkiv, B. Najjari, and J. Ullrich, J. Phys. B **35**, 2205 (2002).
[30] J. Lu, E. Y. Sidky, Z. Roller-Lutz, and H. O. Lutz, Phys. Rev. A **68**, 024702 (2003).
[31] D. Ghosh and C. Sinha, Phys. Rev. A **69**, 052717 (2004).
[32] S. Roy, D. Ghosh, and C. Sinha, J. Phys. B **38**, 2145 (2005).
[33] D. Ghosh and C. Sinha, J. Phys. B **38**, 61 (2005).
[34] M. T. McAlinden, J. E. Blackwood, and H. R. J. Walters, Phys. Rev. A **65**, 032715 (2002).
[35] A. Chattopadhyay and C. Sinha, J. Phys. B **37**, 3283 (2004).
[36] G. N. Watson, *A Treatise on the Theory of Bessel Functions*, 2nd ed. (Cambridge: Cambridge University Press, Cambridge, 1944).
[37] A. Chattopadhyay and C. Sinha, Phys. Rev. A **72**, 053406 (2005).
[38] A. Weingartshofer, J. K. Holmes, G. Caudle, E. M. Clarke, and H. Kruger, Phys. Rev. Lett. **39**, 269 (1977).
[39] A. Weingartshofer, E. M. Clarke, J. K. Holmes, and C. Jung, Phys. Rev. A **19**, 2371 (1979).
[40] N. J. Mason and W. R. Newell, J. Phys. B **20**, 1357 (1987).
[41] N. J. Mason and W. R. Newell, J. Phys. B **22**, 777 (1989).
[42] B. Wallbank, J. K. Holmes, and A. Weingartshofer, J. Phys. B **23**, 2997 (1990).
[43] S. Luan, R. Hippler, and H. O. Lutz, J. Phys. B **24**, 3241 (1991).
[44] B. Wallbank, J. K. Holmes, S. Maclsaac, and A. Weingartshofer, J. Phys. B **25**, 1265 (1992).
[45] B. Wallbank and J. K. Holmes, J. Phys. B **27**, 1221 (1994).
[46] B. Wallbank and J. K. Holmes, J. Phys. B **27**, 5405 (1994).
[47] C. Höhr, A. Dorn, B. Najjari, D. Fischer, C. D. Schröter, and J. Ullrich, Phys. Rev. Lett. **94**, 153201 (2005).
[48] L. I. Schiff, *Quantum Mechanics*, 3rd ed. (McGraw-Hill, New York, 1968), p. 245.